



Investigating the Effect of Hydrostatic Pressure on the Structural, Electronic, Mechanical, Lattice Dynamics and Optical Properties of the Cubic Perovskite RbTaO₃: A DFT Approach

Iyorzor B. E., Babalola M. I. and Ebuwa S.O.

Department of Physics, University of Benin, Nigeria.

Article Info

Keywords: Perovskite, Band gap, Density functional theory (DFT), Semiconductors, Optical functions

Received 07 April 2022

Revised 18 May 2022

Accepted 29 May 2022

Available online 25 June 2022



<https://doi.org/10.37933/nipes.e/4.2.2022.32>

<https://nipesjournals.org.ng>

© 2022 NIPES Pub. All rights reserved

Abstract

Ab-initio calculations based on the spin-polarized density functional theory (SP-DFT) are performed to examine the structural, mechanical, electronic, lattice dynamic and optical properties of the cubic perovskite RbTaO₃ under pressure (0 – 200GPa). The study revealed that the compound is neither ferromagnetic nor non-magnetic from the lattice parameter-energy variation curve. The material is found to be stable and brittle from mechanical stability conditions for cubic structures. The results of the Zener anisotropy factor show that within the pressure range of 0 – 40GPa, the compound is anisotropic while above 40GPa, it portrays isotropic character. It was also observed that it exhibits a semiconductor character as shown in the electronic band structures and the influence of the application of pressure caused the band gap transformation from an indirect band gap at 0GPa to a direct band gap at 150GPa. The existence of this transformation in the energy gap makes RbTaO₃ a promising candidate for optoelectronic, photovoltaic and photochemistry devices applications. From the phonon dispersion curves, it is clear that the material is dynamically unstable due to the presence of negative frequencies. The essential optical functions such as refractive index $n(\omega)$, absorption coefficient spectrum $\alpha(\omega)$, reflectivity $R(\omega)$, electron energy-loss spectrum $L(\omega)$, the extinction coefficient $k(\omega)$ and optical conductivity were investigated. The optical parameters demonstrate that cubic RbTaO₃ is active in visible–ultraviolet regions.

1.0 Introduction

In solid-state inorganic chemistry, the perovskite structural type is one of the most common. The ideal perovskite structure is made up of a three-dimensional framework of corner-sharing BX₆ octahedra and has ABX₃ stoichiometry. The A-site cation is surrounded by 12 equidistant anions and fills the 12 coordinate holes created by the BX₃ network. The perovskite structure can hold majority of the metallic ions from the periodic table as well as a large number of distinct anions. The bulk of perovskite compounds are oxides or fluorides, however the perovskite structure is also known for heavier halides [1]. Also, among ternary oxides, the perovskite is the most prevalent structure and has been researched indepth using the first-principles calculations, and a significant amount of studies in this subject has been re-evaluated because of the oxides' remarkable features. Cubic perovskite solids, on the other hand, crystallize with a space group of $Pm-3m$ (# 221) and are very stable and perfect structure among perovskites. Because of their complex and potentially crucial features, perovskites and their derivatives

have drawn a lot of attention from academics all over the world in recent decades, such as [ferromagnetism [2], superconductivity [3], spin-polarisation [4], colossal magnetoresistance [5], and thermoelectricity [6]. Furthermore, Bouadjemi et al. [7] proposed that the NdMnO₃ perovskite could be a viable spintronic and optoelectronic device material based on their theoretical examination of numerous features, such as structural, magnetic, and optical properties. BaTiO₃ has also been investigated as a possible material for electro-optic devices and ceramic capacitors [8–10]. Ferroelectric ceramics have been employed in microwave devices such as phase shifters, varactors, tunable oscillators, and detectors, and they are the most promising material for electrically tunable devices. [11]. The magnetic and thermoelectric properties of tantalum-based perovskite oxides XTaO₃ (X = Rb, Fr) in cubic phase have been studied [12]. Significant band gap values were observed, namely an indirect energy band gap of 1.12 eV in RbTaO₃ and a direct band gap of 1.08 eV in FrTaO₃. In the work of Madhu et al. [13], the FP-LAPW approach was used to investigate the structural, elastic, and electrical properties of RbTaO₃. The structural features indicate its stability in a perovskite structure. The electronic properties of RbTaO₃ reveal that it has an indirect band gap. The brittle behavior of the current compound was confirmed by the estimated elastic characteristics. The NdInO₃ cubic structure was studied in depth using the density functional theory (DFT) [14]. The study of this material revealed that, due to its large absorption range in the UV area, this material may be ideal for ultraviolet–optical–devices. Using DFT-GGA calculation in the ABINIT code, the structural, electronic and optical properties of Ba_{1-x}Ca_xTiO₃ and Ba_{1-x}Sr_xTiO₃ (x=0.4, 0.6) were investigated [15]. The findings reveal that at M-point, an indirect transition was observed. The relationship between microstructure and dielectric and mechanical losses in Ba_xSr_{1-x}TiO₃ compound was studied. [16]. For phase transitions in Ba_xSr_{1-x}TiO₃, the composition and the size grains affected rate of the loss peak in the dielectric constant/elastic modulus. DFT is used to explore the influence of pressure (0-75GPa) on RbTaO₃ perovskite, and an indirect to direct band gap change is seen [17]. The effects of band gap modification on electrical, optical, and thermoelectric characteristics were investigated. However, in this last report and other literatures on RbTaO₃ perovskite, no information was provided on its structural and lattice dynamic stabilities, also, at what pressure will it become unstable. What magnetic character does it exhibit. In an attempt to address the above issues, we present a study on the effect of hydrostatic pressure on the structural, electronic, mechanical, lattice dynamics and optical properties of the Cubic Perovskite RbTaO₃ by employing the Quantum ESPRESSO package.

2. Computational detail

The QUANTUM ESPRESSO (QE) code's First Principles technique based on (SP-DFT) [18] was used to investigate the various properties. The Projected Augmented Wave Pseudo Potential (PAWPP) was used in the computation [19]. The (GGA) of Perdew-Burke-Ernzerhof (PBE) technique [20] was employed to treat the exchange interaction between electrons, bonding, and magnetic characteristics. Convergence tests for the kinetic energy cut-off and the k-points mesh samplings were carried out before determining their appropriate values for the calculations. The Monkhorst-Pack format with 10x10x10 framework was used, and the kinetic energy cut-off was fixed to 95Ry and convergence thresholds of 10⁻⁸eV/atom for the total energy was used. The Pseudo-atomic configurations adopted as valence electrons are Rb 5s¹, Ta 5d³ 6s² and O 2s² 2p⁴ respectively. The Wyckoff locations of the simple cubic lattices for the compound is shown in Table 1. RbTaO₃ crystallizes in a cubic form, as seen in Figure 1. Rb, Ta, and O atoms are in Wyckoff positions 1a(0,0,0), 1b(1/2,1/2,1/2), and 3c(1/2,1/2,0), respectively, in the *Pm-3m* (221) space group.

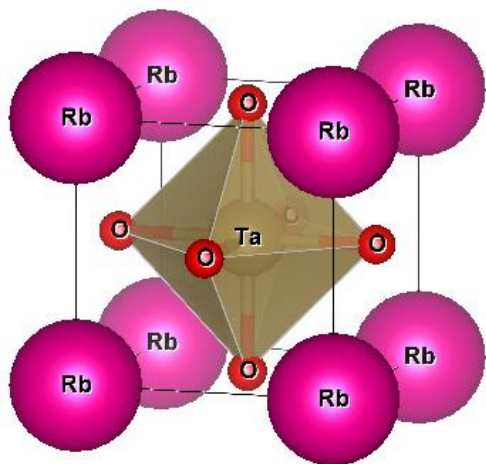


Figure 1. Octahedron structure of RbTaO₃

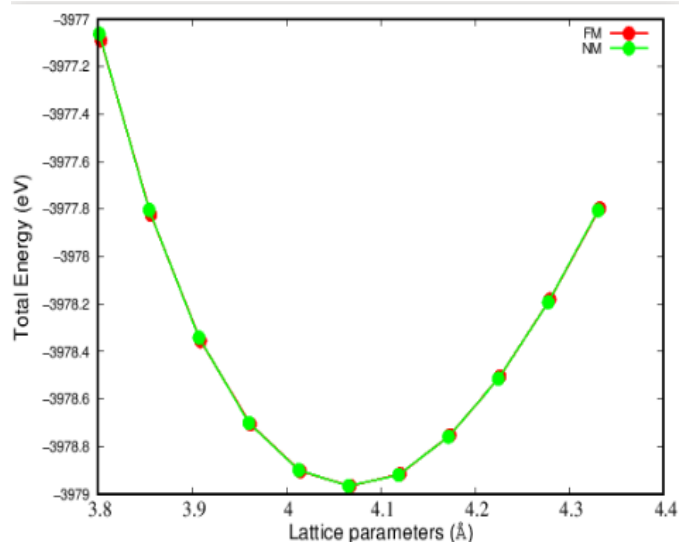


Figure 2. lattice parameters Vs Energy of RbTaO₃

3. Results and Discussion

3.1 Structural and Mechanical Properties

The ground state configuration of the RbTaO₃ perovskite was examined for its structural and mechanical properties. The geometric optimization of the cubic perovskite structure in non-magnetic (NM) and ferromagnetic (FM) states was achieved by total energy minimization of the compound in relation to the modification of the lattice parameters. During the self-consistent computation, the equilibrium lattice constant a , the bulk modulus B , and its pressure derivative B' were obtained and presented in Table 1. Also, the energy-lattice curve for the compound as shown in Figure 2, reveals that the compound is neither ferromagnetic nor non-magnetic. Calculating the tolerance factor 't' of perovskite structures is critical for confirming the geometric stability. In fact, it is an empirical measure that links a perovskite's chemical composition to its stability [21]. The following equation can be used to calculate the Goldschmidt tolerance factor 't' of an ABO₃ perovskite structure.

$$t = \frac{(r_A + r_O)}{\sqrt{2}(r_B + r_O)} \quad (1)$$

where r_A , r_B and r_O are the ionic radii of atoms A, B (cations) and O (anion). The tolerance ranges between $0.8 < t < 1.04$. Another measure for predicting structural stability is the octahedral factor, which is defined as $\mu = r_B/r_O$. The structure is stable when the range of octahedral factor is within $0.414 < \mu < 0.732$ for perovskites. Interestingly, the tolerance factor t and octahedral factor μ for RbTaO₃ are 0.9864 and 0.5151 respectively. These are indications that the compound is stable. Calculating the mechanical stability of materials in solids, the roles of elastic constants and some structural features become inevitable [22]. For cubic phases, the stability is measured by the following criteria $C_{11} + 2C_{12} > 0$, $C_{11} - C_{12} > 0$, $C_{44} > 0$, and $C_{11} > 0$ [23]. From observation, the materials are elastically stable against deformation. To affirm the ductility and brittleness of materials the following factors should be considered; the Poisson's ratio ν , Pugh's index (B/G) and the Cauchy pressure ($C_{12} - C_{44}$) [24, 25]. The bulk B, Young E, and Shear G moduli are important factors for calculating solid mechanical characteristics. The threshold value for distinguishing between ductility

and brittleness of materials is about 1.75 for the B/G ratio [26]. From Table 3, since the B/G ratio values are less than 1.75, it is obvious that the compound is brittle in nature. The Poisson's ratio, which has a value range of 0 to 0.5 [27], reveals the nature of bonding forces in materials. The compound has a high degree of flexibility. Another important structural metric that describes the ductility and brittleness of materials is the Cauchy relation. When the value is positive, the material is said to as ductile; otherwise, it is referred to as brittle. The compound is clearly brittle based on the given data. The results of the Zener anisotropy A, show that the compound is anisotropic within the pressure range of 0GPa to 40GPa, since the values are approaching unity. This is an indication of high elastic anisotropy, while above 40GPa it portrays isotropic character.

Table 1. The Structural properties: the a (Å), B (GPa), band gap near Fermi energy E_g (eV) and bond length B_L (Å) within pressure range of (0 – 200) (GPa)

	0GPa	10GPa	20GPa	30GPa	40GPa	50GPa	75GPa	100GPa	150GPa	200GPa
a	4.0678	3.9884	3.9354	3.8905	3.8518	3.8169	3.7444	3.6851	3.5920	3.5200
B	182.60	220.95	259.82	294.57	327.05	357.24	432.83	507.54	641.31	772.48
E_g	2.0534	2.1837	2.2675	2.3361	2.3933	2.4420	2.5359	2.6034	2.6720	2.7014
B_L	2.0330	1.9943	1.9679	1.9454	1.9258	1.9085	1.8721	1.8426	1.7961	1.7599

From Table 1 and Figure 3(a-c), it is clear that the lattice constant and bond length are inversely proportional to the pressure, while the elastic constants, bulk modulus and the energy band gap are directly proportional to the pressure.

3.2 Electronic Properties

The calculated electronic band structures of the Cubic Perovskite RbTaO_3 under the effect of hydrostatic pressure (0 – 200GPa) are purely semiconductors with the Fermi energy level located at the maximum valence band. Considering the extreme of the pressures, for the 0GPa, the highest occupied valence band is located at M-point and the lowest unoccupied one in the conduction band is located at Γ -point, indicating an indirect band gap of 2.0534eV. For 150GPa, both the highest occupied valence band and the lowest unoccupied conduction band are all located at Γ -point, indicating a direct band gap of 2.672eV. As the pressure increases beyond 150GPa a transition from indirect to a direct band gap started manifesting, and this transformation became very obvious at 150GPa as presented in Figure 4(a and b).

In the work of Hassan et al. [17], the band structure for RbTaO_3 was computed using mBJ potential as implemented in Wien2K, at $P = 0\text{GPa}$ an indirect band gap was obtained and at $P = 75\text{GPa}$ a direct band gap was obtained. The transformation occurred at 75GPa, rather than the 150GPa reported in this paper, due to the use of PBE-GGA functional as implemented in the Quantum ESPRESSO code. The existence of this transformation in the energy gap makes RbTaO_3 a promising candidate for optoelectronic, photovoltaic and photochemistry devices applications. To be considered for photovoltaic and photochemistry, semiconductors must have an optimal band gap more than 1.4 and less than 3.0 eV [28]. The partial density of states (PDOS) for the various pressures of the compound have also been calculated and shown in Figures 5(a-b). The purpose of the PDOS plot is to shed light on the type of bonding between the orbitals and the effect of individual orbitals on the DOS.

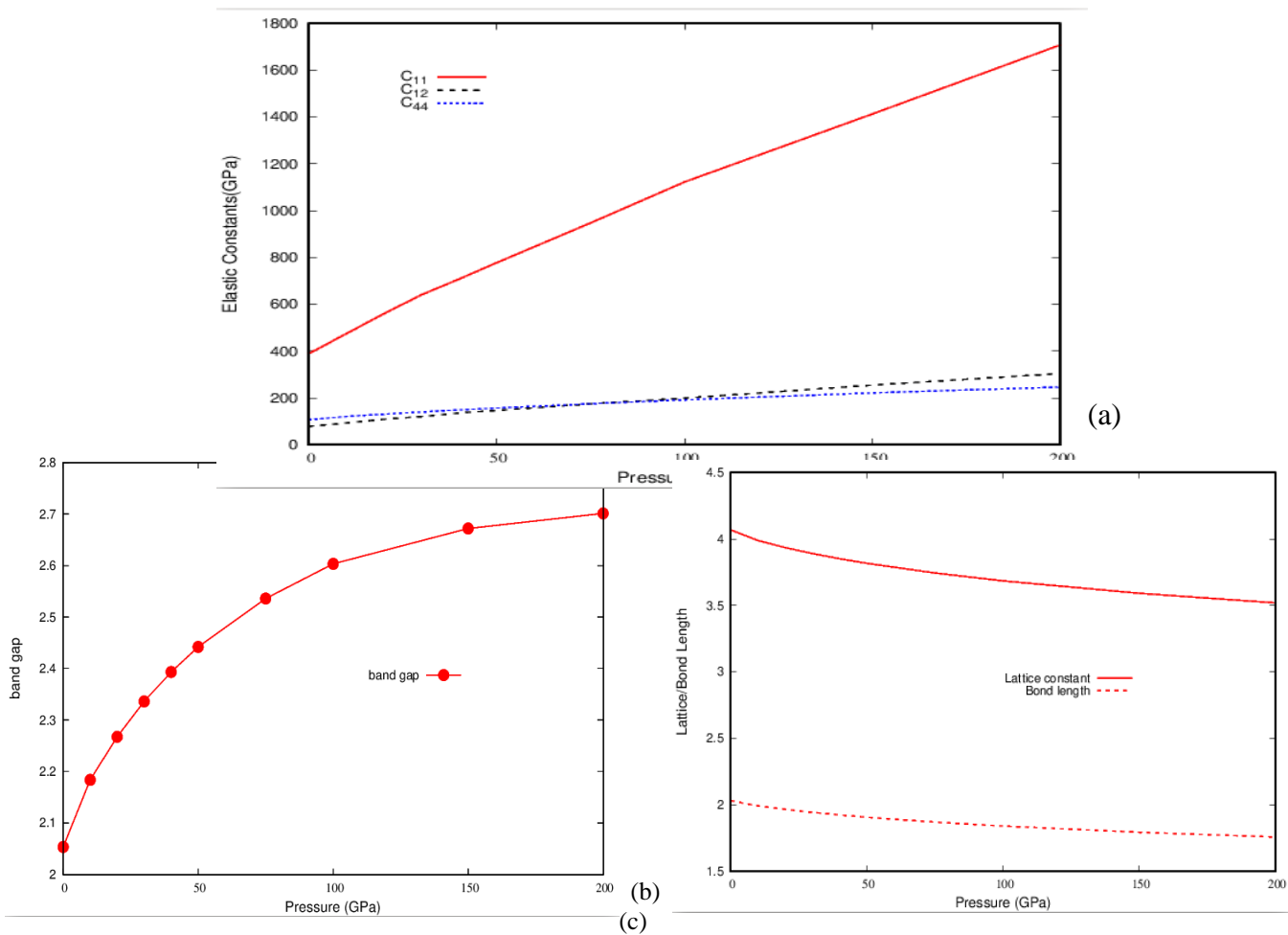


Figure 3(a-c): (a) Pressure vs Elastic constants, (b) Pressure vs band gap, (c) Pressure vs Lattice/bond length

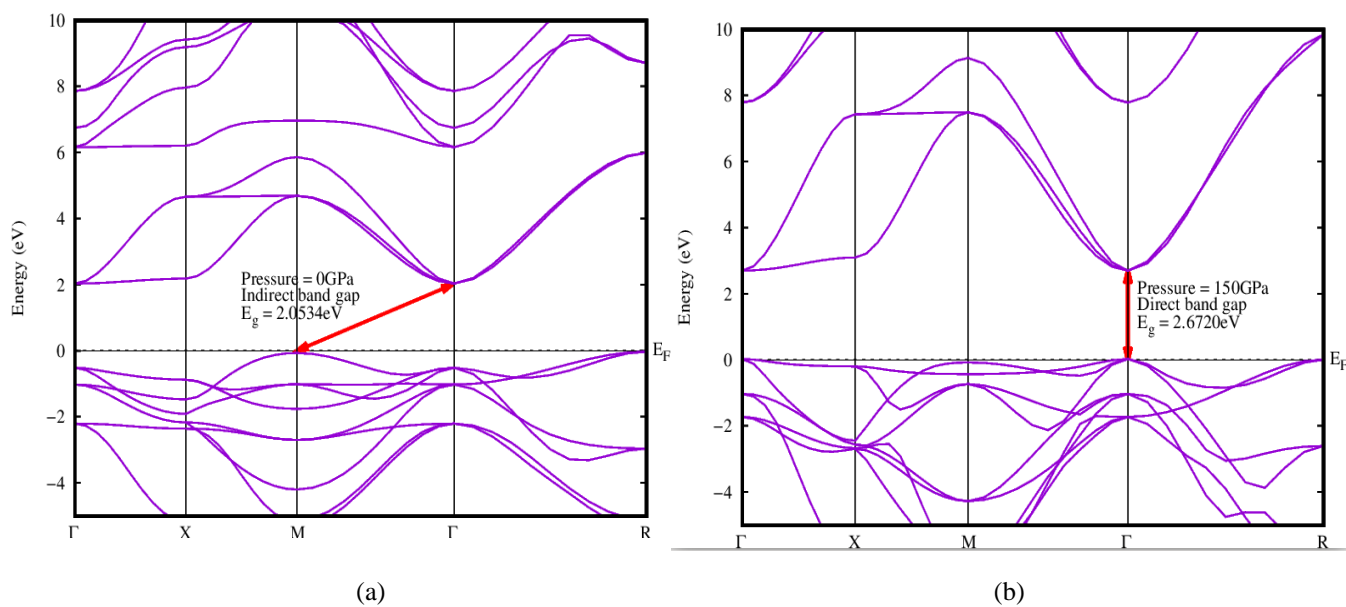


Figure 4. Electronic band structures of RbTaO₃ for pressures

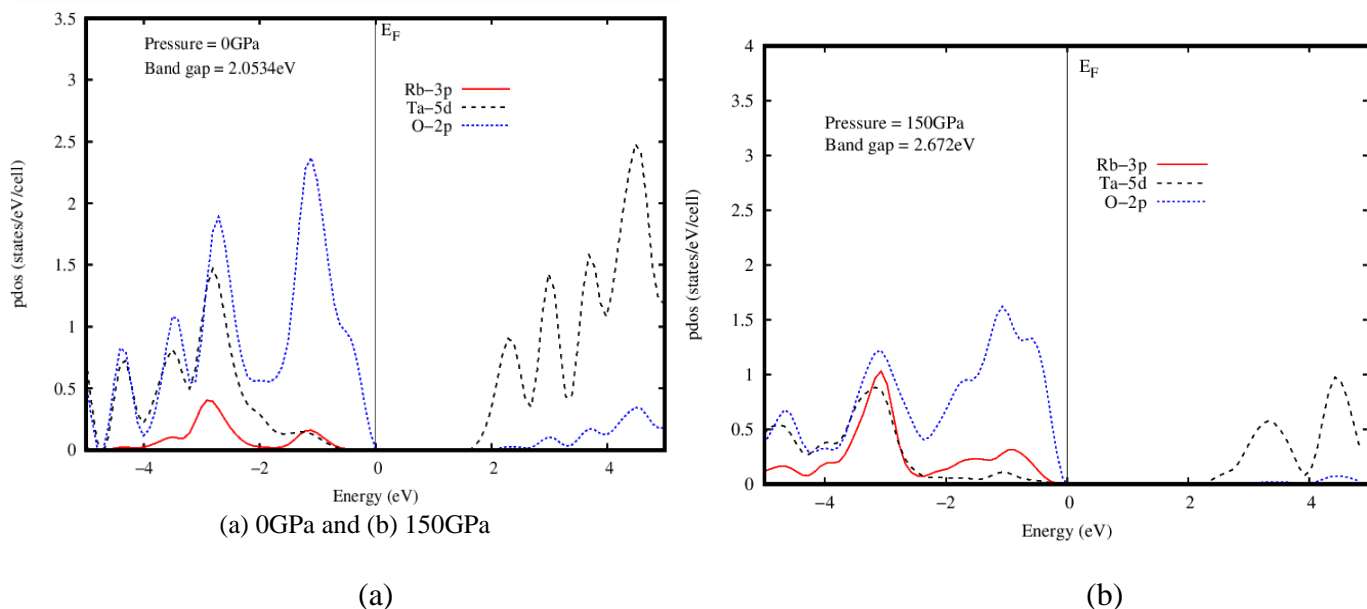


Figure 5. The PDOS of RbTaO₃ for pressures (a) 0GPa and (b) 150GPa

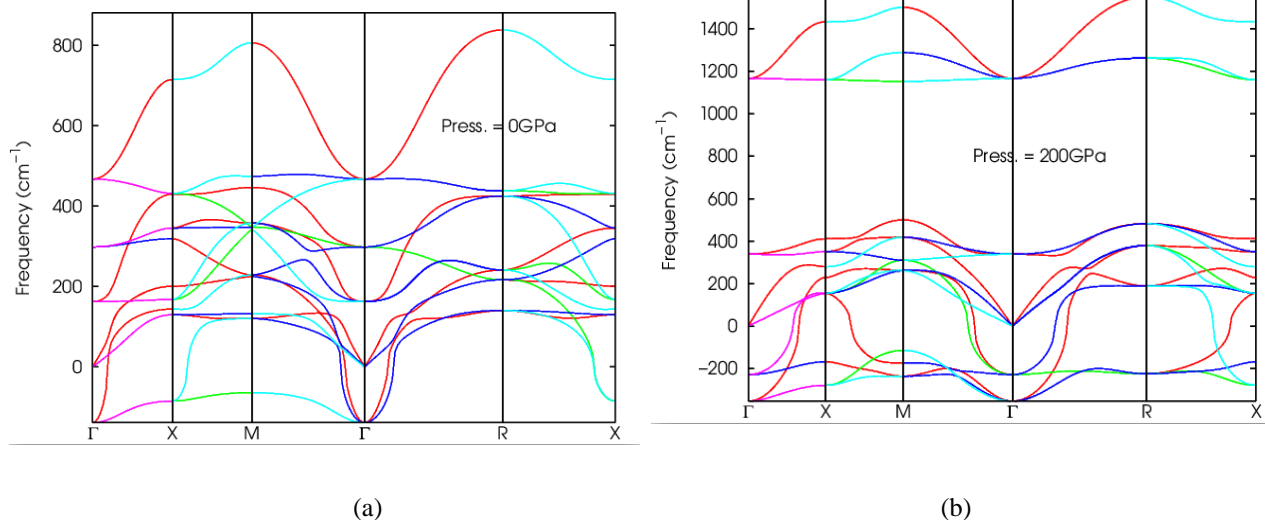


Figure 6(a-b) Phonon dispersion curves along symmetry directions of RbTaO₃ at pressure (0GPa and 200GPa)

At 0GPa, within the conduction band, the major contribution originated from the Ta-5*d* orbital and little from the O-2*p* orbital. Their effect is far from the Fermi energy level, it started from about 1.9eV. Similarly, in the valence band, the three orbitals made their individual contributions, with O-2*p* orbital having the highest contribution and the least from Rb-3*p* orbital. There was a deterioration in the maxima of all the hybridized orbitals at 200GPa pressure. It was discovered that there existed a strong covalent bond. Except for the Ta-5*d* orbital, the orbital contribution decayed almost completely in the conduction band. The repulsive force between atoms increased as a result of the high pressure. The band gap between the valence and conduction bands widened as a result.

3.3. Vibrational properties

To examine the vibrational properties of RbTaO₃ compound, the phonon spectra of the various pressures (0-200GPa) were computed. We used the Thermo_pw package, which is a code that uses Quantum ESPRESSO routines as the underlying engine to compute the physical properties of materials. Figure 6(a – b) shows the phonon dispersion curves along the $\Gamma - X - M - \Gamma - R - X$ high symmetry directions. One notable aspect was the discovery of imaginary (negative) frequencies in the compound's Brillouin zone, indicating that it is dynamically unstable.

3.4 Optical properties

The optical properties of the RbTaO₃ compound under hydrostatic pressure in the 0–18.4eV range are presented in Figures 7(a-g). The optical characteristics are calculated using the complex dielectric function $\varepsilon(\omega) = \varepsilon_1(\omega) + i\varepsilon_2(\omega)$, where $\varepsilon(\omega)$ represents the interaction of incoming radiation with matter. The complex dielectric function describes the linear response of a system to external electromagnetic radiation. The momentum matrix elements between the occupied and unoccupied wave functions are used to calculate the dispersion of the imaginary part of the complex dielectric function $\varepsilon_2(\omega)$, and the real part of the dielectric function $\varepsilon_1(\omega)$ is calculated using the Kramers–Kronig transformation [29]. The real part of the dielectric constant, which is the electronic part of the static dielectric constant, is an important quantity in the zero frequency limits. The static dielectric constants are 5.62, 5.36, 5.33 and 5.38 for 0GPa, 50GPa, 150GPa and 200GPa respectively. Furthermore, increasing the pressure above 0GPa suppresses the entire $\varepsilon_1(\omega)$ spectrum, it decays with pressure. These results are in close agreement when compared with the literature [17]. The maximum peak in the imaginary part of the dielectric function $\varepsilon_2(\omega)$ spectra of the compound at 0GPa occur at 5.38eV, 50GPa at 11.69eV, 150GPa at 12.62eV, and 200GPa occur at 13.54eV respectively, and then decreases linearly with the increasing pressure. With rising external pressure, the imaginary dielectric constant $\varepsilon_2(\omega)$ exhibits higher energy shifts.

The fundamental optical functions, such as refractive index $n(\omega)$, absorption coefficient spectrum $\alpha(\omega)$, reflectivity $R(\omega)$, electron energy-loss spectrum $L(\omega)$, the extinction coefficient $k(\omega)$ and optical conductivity can be calculated by understanding the real and imaginary parts of the dielectric function. The absorption coefficient is a key component since it informs us about the best solar energy conversion efficiency and reveals how much light of a specific energy or frequency may pass through a material before it is absorbed. The absorption coefficient describes the intensity attenuation of the light passing through a material. It can be understood as the sum of the absorption cross-sections per unit volume of a material for an optical process. For 0GPa and 200GPa, the absorption coefficient increased from 2.78eV, up to 6.12eV, and then declined slightly before increasing sharply from 6.12eV to 18.37eV. The highest peaks for 0GPa and 200GPa are $30.79(\omega)$ and $59.54(\omega)$, respectively, see Figure 7(d). The RbTaO₃ seems to have a good absorption coefficient since it has a wide range of about 5eV-16eV and occurring at low energy region. The absorption coefficient is enhanced with increase in pressure. Figure 7(e) shows the computed reflectivity $R(\omega)$ of the investigated compound within (0 - 18 eV). The reflectivity of the incident radiation attains its peak close to 32.7% at 5.9eV and 40.7% at 15.8eV for 0GPa and 200GPa respectively. This implies that about 32.7% of the incident radiation is reflected and 67.3% can be absorbed within the ultra-violet (UV) region. From the graph, the reflectivity $R(0)$, at zero frequency reduces with pressure. The calculated refractive index $n(\omega)$ is presented in Figure 7c. At zero frequency limit, the static refractive indexes $n(0)$ values are 2.37 and 2.32 for 0GPa and 200GPa respectively. The electron energy loss function, $L(\omega)$ is a critical optical

characteristic that indicates the potential for rapid electron interactions inside a material. These interactions are responsible for intraband transitions, phonon excitation, inner shell ionizations, and plasmon excitations in addition to interband transitions [30]. In Figure 7(g), the $L(\omega)$ shows three sharp peaks, at 6.31eV, 14.29eV and 17.99eV for 0GPa. While for 200GPa, the two major peaks are located at 10.02eV and 17.25eV. The peaks are mainly around the ultra-violet regions. The computed $L(\omega)$ is minimum in the infrared, visible, and lower ultraviolet regions, implying that RbTaO₃ has optical uses. As the amplitude of the energy loss function increases at higher energies, the imaginary part of the dielectric function gets smaller. The computation reveals that, increase in pressure results in lower frequencies of the energy loss. The attenuation of electromagnetic waves in materials is described by the extinction coefficient $k(\omega)$. The calculated extinction coefficient $k(\omega)$ for RbTaO₃ at 0GPa - 200GPa are displayed in Figure 7(f). Within the visible light region, the value of $k(\omega)$ increases from 0.22 – 0.82 with energy and reached a maximum value of 1.69 at 5.75eV in the UV region. The value of $k(\omega)$ starts decaying and inactive in the high energy region, and frequencies of $k(\omega)$ are enhanced with increase in pressure of the compound.

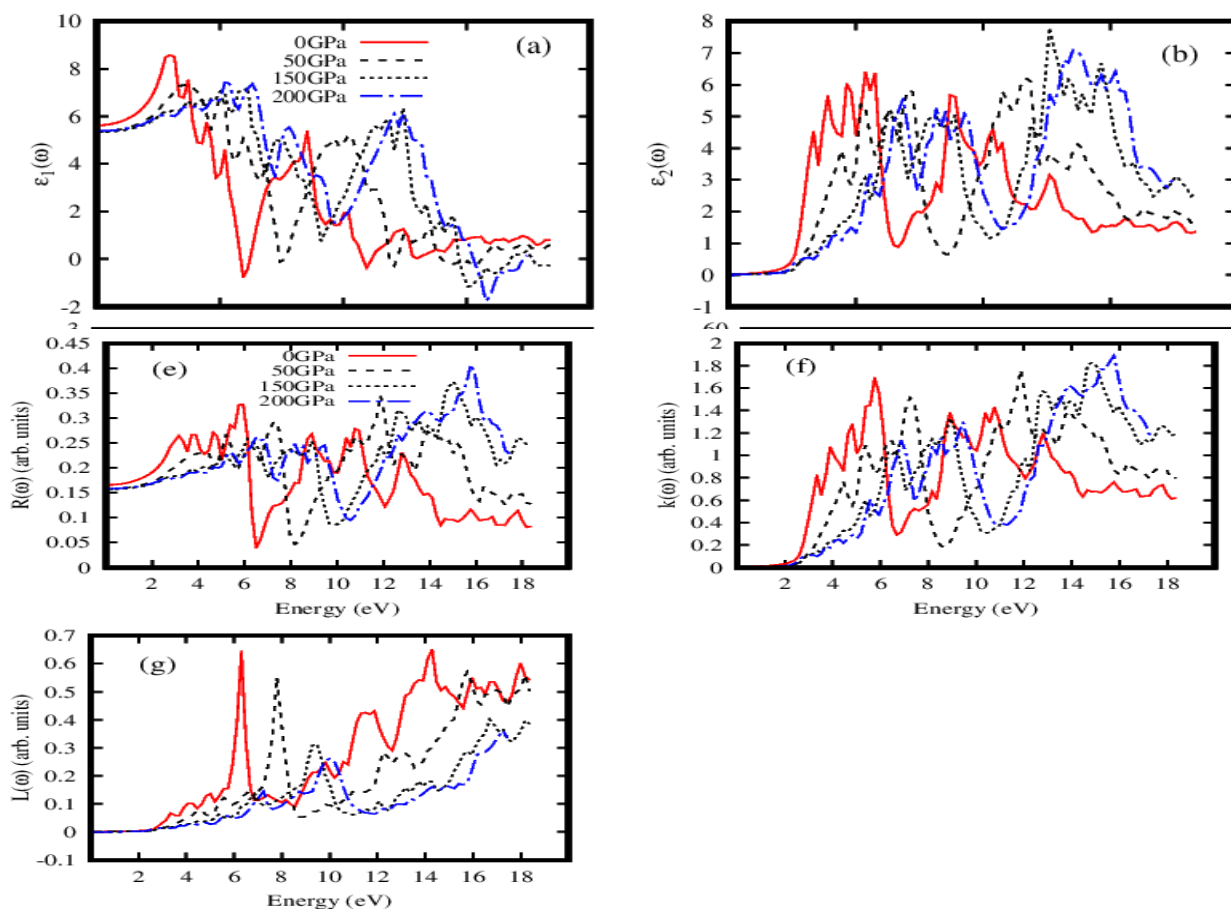


Figure 7(a-g): (a) Real part of the dielectric function $\epsilon_1(\omega)$, (b) Imaginary part of the complex dielectric function $\epsilon_2(\omega)$, (c) refractive index $n(\omega)$, (d) absorption coefficient spectrum $\alpha(\omega)$, (e) reflectivity $R(\omega)$, (f) the extinction coefficient $k(\omega)$ (g) electron energy-loss spectrum $L(\omega)$.

4.0. Conclusion

We have investigated and presented the effect of hydrostatic pressure (0GPa – 200GPa) on the structural, electronic, mechanical, lattice dynamics and optical properties of the Cubic Perovskite RbTaO₃ using First Principles calculations as implemented in the QUANTUM ESPRESSO code. Firstly, the tolerance factor ‘*t*’ and the octahedral factor ‘*μ*’ which are empirical measures that links the perovskite RbTaO₃ chemical composition to its stability were investigated. The results for ‘*t*’ and ‘*μ*’ satisfy the requirements, hence the compound is considered to be structurally stable. Mechanically, from the values of the B/G ratio and Cauchy relation the material is found to be brittle. Also, it is elastically stable against deformation from the elastic constants criteria. The results of the Zener anisotropy factor show that within the pressure range of 0 – 40GPa, the compound is anisotropic while above 40GPa, it portrays isotropic character. And the results of the bulk modulus reveal that as the pressure increases beyond 40GPa the material becomes very hard. It was found that the electronic band structures of the compound under pressure are purely semiconductors. A transformation from indirect to a direct band gap was observed as the pressure increases beyond 150GPa. Couple with the fact that the energy band gaps fall within the range of 1.4eV to 3.0eV, the RbTaO₃ compound is a good contender for optoelectronic, photovoltaic and photochemistry devices applications [28]. The lattice dynamics of the compound was investigated with the use of Thermo_pw code and imaginary (negative) frequencies in the Brillouin zone was observed. This feature reveals that it is dynamically unstable. The various optical quantities are also calculated and discussed. The optical band gaps from the absorption coefficient spectrum are found to be close to the energy band gap of the material.

References

- [1] Lufaso, M. W., and Woodward, P. M. (2001). Prediction of the crystal structures of perovskites using the software program SPuDS. *Acta Crystallographica Section B: Structural Science*, 57(6), 725-738.
- [2] Khandy, S. A., & Gupta, D. C. (2017). Structural, elastic and magneto-electronic properties of half-metallic BaNpO₃ perovskite. *Materials Chemistry and Physics*, 198, 380-385.
- [3] Schneemeyer, L. F., Waszczak, J. V., Zahorak, S. M., van Dover, R. B., & Siegrist, T. (1987). Superconductivity in rare earth cuprate perovskites. *Materials research bulletin*, 22(11), 1467-1473.
- [4] El Rhazouani, O., Zahrri, Z., Benyoussef, A., & El Kenz, A. (2016). Magnetic properties of the fully spin-polarized Sr₂CrOsO₆ double perovskite: A Monte Carlo simulation. *Physics Letters A*, 380(13), 1241-1246.
- [5] Raveau, B., Maignan, A., Martin, C., & Hervieu, M. (1998). Colossal magnetoresistance manganite perovskites: relations between crystal chemistry and properties. *Chemistry of materials*, 10(10), 2641-2652.
- [6] Reshak, A. H. (2016). Transport properties of the n-type SrTiO₃/LaAlO₃ interface. *RSC Advances*, 6(95), 92887-92895.
- [7] Bouadjemi, B., Bentata, S., Abbad, A., & Benstaali, W. (2015). Ab-initio study of optoelectronic and magnetic properties of the orthorhombic NdMnO₃ perovskite. *Solid State Communications*, 207, 9-15.
- [8] Pithan, C., Hennings, D., & Waser, R. (2005). Progress in the synthesis of nanocrystalline BaTiO₃ powders for MLCC. *International Journal of Applied Ceramic Technology*, 2(1), 1-14.
- [9] Tian, Z., Wang, X., Shu, L., Wang, T., Song, T. H., Gui, Z., & Li, L. (2009). Preparation of nano BaTiO₃-based ceramics for multilayer ceramic capacitor application by chemical coating method. *Journal of the American Ceramic Society*, 92(4), 830-833.
- [10] Tsurumi, T., Adachi, H., Kakemoto, H., Wada, S., Mizuno, Y., Chazono, H., & Kishi, H. (2002). Dielectric properties of BaTiO₃-based ceramics under high electric field. *Japanese journal of applied physics*, 41(11S), 6929.
- [11] Jindal, S., Vasishth, A., Devi, S., & Anand, G. (2018). A review on tungsten bronze ferroelectric ceramics as electrically tunable devices. *Integrated Ferroelectrics*, 186(1), 1-9.
- [12] Hussain, M. I., Khalil, R. A., Hussain, F., & Rana, A. M. (2021). DFT-based insight into the magnetic and thermoelectric characteristics of XTaO₃ (X= Rb, Fr) ternary perovskite oxides for optoelectronic applications. *International Journal of Energy Research*, 45(2), 2753-2765.
- [13] Sarwan, M., Shukla, P., & Singh, S. (2020). Structural stability, electronic and elastic properties of cubic RbTaO₃ perovskite oxide. In *AIP Conference Proceedings* (Vol. 2265, No. 1, p. 030341). AIP Publishing LLC.

- [14] Butt, M. K., Yaseen, M., Ghaffar, A., & Zahid, M. (2020). First principle insight into the structural, optoelectronic, half metallic, and mechanical properties of cubic perovskite NdInO₃. *Arabian Journal for Science and Engineering*, 45(6), 4967-4974.
- [15] Tahiri, O., Kassou, S., & Mrabet, R. (2018). First principles calculations of electronic and optical properties for mixed perovskites: Ba (1-x) Ca (x) TiO₃ and Ba (1-x) Sr (x) TiO₃ (x= 0.4, 0.6). *Materials and Devices*, 3, 2004-2018.
- [16] Cheng, B. L., Su, B., Holmes, J. E., Button, T. W., Gabbay, M., & Fantozzi, G. (2002). Dielectric and mechanical losses in (Ba, Sr) TiO₃ systems. *Journal of electroceramics*, 9(1), 17-23.
- [17] Hassan, M., Liaqat, M., & Mahmood, Q. (2021). Pressure dependence of electronic, optical and thermoelectric properties of RbTaO₃ perovskite. *Applied Physics A*, 127(4), 1-8.
- [18] Giannozzi, P., Baroni, S., Bonini, N., Calandra, M., Car, R., Cavazzoni, C., Ceresoli, D., Chiarotti, G.L., Cococcioni, M., Dabo, I. and Dal Corso, A., (2009). *Journal of physics: Condensed matter*, 21(39), p.395502.
- [19] Perdew JP, Burke K, Ernzerhof M. (1996). Generalized gradient approximation made simple. *Phys. Rev. Lett.* 77, 3865–3868.
- [20] Perdew JP, Burke K, Ernzerhof M. (1997). Generalized gradient approximation made simple. *Phys. Rev. Lett.* 78, 1396.
- [21] Ilyas, A., Khan, S. A., Liaqat, K., & Usman, T. (2021). Investigation of the structural, electronic, magnetic, and optical properties of CsXO₃ (X= Ge, Sn, Pb) perovskites: A first-principles calculations. *Optik*, 244, 167536.
- [22] Wu, Z., Hao, X., Liu, X. and Meng, J. (2007). *Phys. Rev. B.* 75(5), 054115.
- [23] Sin'ko G. V. and Smirnow N. A. (2002). *J. Phys. Condens. Matter* 14, 6989.
- [24] Iyorzor B. E., Babalola M. I., Adetunji B. I. and Bakare F. O. (2018). Effect of Tellurium333 concentration on the structural, electronic and mechanical properties of Beryllium Sulphide: DFT approach. *Materials Research Express*, 5(5), 056517.
- [25] Bakare F. O., Babalola M. I. and Iyorzor B. E. (2017). *Materials Research Express*, 4(11), 116502.
- [26] Pugh S. F. :The London, Edinburgh, and Dublin Philosophical Magazine and journal of science, 45 (367), 823-843, (1954).
- [27] Boucetta S. (2014). *Journal of Magnesium and Alloy* 2, 59.
- [28] L. Azzouz , M. Halit , M. Rerat, R. Khenata, A. K. Singh, M. M. Obeid, H. R. Jappor and X. Wang (2019). Structural, electronic and optical properties of ABTe₂ (A= Li, Na, K, Rb, Cs and B= Sc, Y, La): Insights from first-principles computations. *Journal of Solid State Chemistry*, 279, 120954.
- [29] Hu, J. M., Huang, S. P., Xie, Z., Hu, H., & Cheng, W. D. (2007). First-principles study of the elastic and optical properties of the pseudocubic Si₃As₄, Ge₃As₄ and Sn₃As₄. *Journal of Physics: Condensed Matter*, 19(49), 496215.
- [30] Murtaza, G., Gupta, S. K., Seddik, T., Khenata, R., Alahmed, Z. A., Ahmed, R., Khachai H, Jha P. K. and Omran, S. B. (2014). Structural, electronic, optical and thermodynamic properties of cubic REGa₃ (RE= Sc or Lu) compounds: Ab initio study. *Journal of alloys and compounds*, 597, 36-44.